A Wavelet-Based Multiresolution Regularized Least Squares Reconstruction Approach for Optical Tomography

Wenwu Zhu, Yao Wang,* *Member, IEEE*, Yining Deng, Yuqi Yao, and Randall L. Barbour, *Member, IEEE*

Abstract—In this paper, we present a wavelet-based multigrid approach to solve the perturbation equation encountered in optical tomography. With this scheme, the unknown image, the data, as well as the weight matrix are all represented by wavelet expansions, thus yielding a multiresolution representation of the original perturbation equation in the wavelet domain. This transformed equation is then solved using a multigrid scheme, by which an increasing portion of wavelet coefficients of the unknown image are solved in successive approximations. One can also quickly identify regions of interest (ROI's) from a coarse level reconstruction and restrict the reconstruction in the following fine resolutions to those regions. At each resolution level a regularized least squares solution is obtained using the conjugate gradient descent method. This approach has been applied to continuous wave data calculated based on the diffusion approximation of several two-dimensional (2-D) test media. Compared to a previously reported one grid algorithm, the multigrid method requires substantially shorter computation time under the same reconstruction quality criterion.

Index Terms—Image reconstruction, multigrid method, optical tomography, wavelet transform.

I. INTRODUCTION

RECENTLY, there has been a growing interest and rapid progress in developing medical optical imaging systems which use near-infrared light emitted into human tissue to determine the interior optical properties [1]. Interest remains high because the method appears to offer several important advantages over other established imaging modalities. These include the use of nonionizing sources and highly sensitive detectors, the ability to monitor situations and events critical to sustaining life (e.g., tissue oxygenation), and the availability of compact, low-cost instrumentation that can be made portable.

W. Zhu and Y. Yao were with the Department of Electrical Engineering, Polytechnic University, Brooklyn, NY 11203 USA. They are now with Bell Labs., Lucent Technologies, Whippany, NJ 07981 USA.
*Y. Wang is with the Department of Electrical Engineering, Polytechnic University, Brooklyn, NY 11201 USA (e-mail: yao@vision.poly.edu).
Y. Deng was with the Department of Electrical Engineering, Polytechnic University, Brooklyn, NY 11201 USA. He is now with the Department of Electrical Engineering, University of California, Santa Barbara, CA 93106 USA.
R. L. Barbour is with the Departments of Pathology and Biophysics, SUNY Health Science Center, Brooklyn, NY 11203 USA.

The problem is difficult because in this frequency range, photons propagate through the tissue in a highly diffused manner and the relation between the measured signal and the absorption properties of the medium is nonlinear. There is generally no direct method for solving the inverse problem. One way to attack this difficulty is to use the *iterative perturbation approach* which entails solving a system of linear equations at each iteration, that computes the difference in optical properties between the target (unknown) medium and a defined reference medium. More specifically, it was described by some of us using both the transport [2], [3] and diffusion [4] models of the light propagation. Independently, Singer *et al.* [5] and Arridge *et al.* [6], [7] described alternative iterative schemes derived from random walk and diffusion theory. All these schemes require, at each perturbation step, the solution of a linear perturbation equation of the following form:

$$Hx = y \tag{1}$$

where x is an $L \times 1$ vector of differences between the optical properties (such as absorption and scattering coefficients) of a reference medium and those of the imaged medium in L voxels, y is a $K \times 1$ vector of changes in K detector readings between the two media, and H is a $K \times L$ matrix of weights, each describing the influence of a voxel on a detector reading, which is equal to the derivative of the detector reading with respect to the optical properties at the voxel in the reference medium. In general, the perturbation equation is both underdetermined and ill posed. To solve the linear perturbation equation, we have developed several iterative algorithms, including projection onto convex sets (POCS) [2], conjugate gradient descent (CGD) [2], multigrid reconstruction [2], layer stripping [8], [9] [for time-resolved (TR) data], regularized least squares (RLS) [9], and total least squares (TLS) [10].

One challenging problem in solving the perturbation equation is that the computation complexity is usually very high due to the extremely large dimension of the weight matrix. One effective way to speedup the solution of a linear system is by using a multigrid approach. In general, such an approach first represents the original system equation at successively coarser resolutions, and then solves the equation from the coarse levels to the fine levels. There are many ways one can deduce a multiresolution representation of a given linear system. Recently, several researchers have investigated the use of wavelet transforms for such a task. In [11], Wang *et al.*

proposed a RLS-based multigrid algorithm for image restoration using wavelet expansion. In [12], Delaney *et al.* proposed a wavelet-based multiresolution tomographic reconstruction algorithm [filtered back projection (FBP)-based] for emission tomography. In this paper, we explore the use of wavelet-based multigrid reconstruction in optical tomography. In our approach, a multiresolution representation of the perturbation equation is obtained by expanding the unknown, the data, and the weight matrix using wavelet bases. The transformed equation is then solved from coarse to fine resolutions using the solution obtained from the previous resolution as the initial solution in the present resolution. Compared to a one-grid method which solves the equation in the finest resolution directly, the computational complexity is reduced significantly under the same reconstruction quality criterion.

II. WAVELET MULTIRESOLUTION REPRESENTATION

A. 1-D Discrete Signal Wavelet Representation

The theory of multiresolution decomposition of a signal by a family of orthonormal wavelets can be found in [13]. In this study, we use discrete wavelet transform to represent a discrete signal. For a discrete signal with K samples the wavelet transform can be represented in the following matrix form:

$$\tilde{f} = Wf \tag{2}$$

where $f = [f(x_1), f(x_2), \cdots, f(x_K)]^T = [f_1, f_2, \cdots, f_K]^T$ consists of discrete samples of the original signal, $\tilde{f} = [\tilde{f}_1, \tilde{f}_2, \cdots, \tilde{f}_K]^T$ consists of wavelet transform coefficients, and W is an $K \times K$ transform matrix in which each row vector corresponds to a transform basis vector. The wavelet transform base is designed so that the transformed coefficients can be grouped into two subsignals consisting of an approximation signal $A_{-1}f$ and a detail signal $D_{-1}f$, each of dimension $K/2$. We can further decompose the approximation signal $A_{-1}f$ into an approximation signal $A_{-2}f$ and a detail signal $D_{-2}f$. This yields a three-level wavelet-based multiresolution representation of f as

$$\tilde{f}_{(K \times 1)} = A_0 f_{(K \times 1)} = \begin{bmatrix} A_{-1}f_{(K/2 \times 1)} \\ D_{-1}f_{(K/2 \times 1)} \end{bmatrix} = \begin{bmatrix} A_{-2}f_{(K/4 \times 1)} \\ D_{-2}f_{(K/4 \times 1)} \\ D_{-1}f_{(K/2 \times 1)} \end{bmatrix}.$$

In the above equation, the subscript in parenthesis describes the dimension of the associated matrix. The approximation signal can be repeatedly split in such a way to yield an arbitrary $L \leq \log_2 K$ level representation.

B. 2-D Signal Wavelet Representation

An efficient way of implementing a wavelet transform of a two-dimensional (2-D) image is as follows: first apply a one-dimensional (1-D) transform to each row of the 2-D image and then apply a 1-D wavelet transform to each column. This is known as separable wavelet transform.

Let F represent a 2-D image with size $M \times N$ and let f be the vector consisting of elements of F arranged in the lexicographic order, with size $K = M \times N$. Let W_M and W_N represent the 1-D wavelet-transform matrix of size $M \times M$ and $N \times N$, respectively, the separable wavelet transform of F can be described by

$$\tilde{F} = W_M F W_N^T \tag{3}$$

where T denotes transpose. This is equivalent to, in the 1-D notation

$$\tilde{f} = (W_M \otimes W_N)f \tag{4}$$

where $\otimes$ denotes the Kronecker product and $\tilde{f}$ is the vector consisting of elements of $\tilde{F}$ arranged in the lexicographic order. Therefore, performing 2-D wavelet transform to a $M \times N$ 2-D image using separable transform is equivalent to performing 1-D wavelet transform to the corresponding 1-D vector by using $W_K = W_M \otimes W_N$. The transformed image can be grouped into four subimages consisting of an approximation image $A_{-1}F$ and three detail subimages D_{-1}^1F, D_{-1}^2F, and D_{-1}^3F, i.e.,

$$\tilde{F}_{(M \times N)} = \begin{bmatrix} A_{-1}F_{(M/2 \times N/2)} & D_{-1}^1F_{(M/2 \times N/2)} \\ D_{-1}^2F_{(M/2 \times N/2)} & D_{-1}^3F_{(M/2 \times N/2)} \end{bmatrix}.$$

This is a two-level representation of F and can be implemented by a set of quadrature mirror filters (QMF's) illustrated in Fig. 1 (2-levels). Usually we refer to them as LL, LH, HL, and HH subimages—where LL represents low frequencies in horizontal and vetical directions, LH represents low frequency in horizontal direction and high frequency in vertical direction, HL represents high frequency in horizontal direction and low frequency in vertical direction, and HH represents high frequencies in horizontal and vertical directions. One can continue to decompose the subimage $A_{-1}F$ further to the next scale (coarser resolution), which leads to the three-level representation shown at the bottom of the page. One can repeatedly apply the wavelet transform to the approximation subimage to obtain an $L \leq \min\{\log_2 M, \log_2 N\}$ level representation.

III. SOLUTION OF THE PERTURBATION EQUATION IN THE WAVELET DOMAIN

A. 1-D Wavelet Representation of the Perturbation Equation

Considering the perturbation equation in (1). To represent the perturbation equation in a wavelet domain, let the transform matrices for x and y be represented by W_x and W_y, respectively. Assuming the transformation matrix W_x

$$\tilde{F}_{(M \times N)} = \begin{bmatrix} A_{-2}F_{(M/4 \times N/4)} & D_{-2}^1F_{(M/4 \times N/4)} & \\ & & D_{-1}^1F_{(M/2 \times N/2)} \\ D_{-2}^2F_{(M/4 \times N/4)} & D_{-2}^3F_{(M/4 \times N/4)} & \\ & D_{-1}^2F_{(M/2 \times N/2)} & D_{-1}^3F_{(M/2 \times N/2)} \end{bmatrix}$$

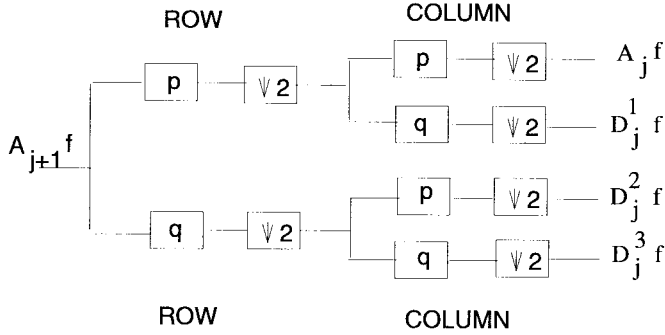Fig. 1.　Wavelet decomposition of 2-D image from level $j + 1$ to j.

FWT: Forward Wavelet Transform
IWT: Inverse Wavelet Transform

Fig. 2.　Modified V-cycle multigrid algorithm.

is orthonormal, and multiplying (1) from left by W_y and inserting $W_x^T W_x = I$ in between H and x, we obtain

$$\tilde{H}\tilde{x} = \tilde{y} \tag{5}$$

where $\tilde{H} = W_y H W_x^T$, $\tilde{y} = W_y y$, and $\tilde{x} = W_x x$. Equation (5) is the perturbation equation in the wavelet domain. From this equation, one can solve $\tilde{x}$, and then obtain x by an inverse transform $x = W_x^T \tilde{x}$.

B. RLS Solution in Wavelet Domain

Regularization is a well-established technique for dealing with instability in inverse problems [14] and can convert an ill-posed problem into a well-posed problem by incorporating *a priori* knowledge about the image to be recovered. RLS can be formulated as

$$\hat{x} = \arg\min_x \{\|Hx - y\|^2 + \lambda\|x\|^2\} \tag{6}$$

where the *regularization parameter* λ can be determined by the Miller criterion [15] or Cross-validation method [16]. The RLS solution is given by

$$\hat{x} = (H^T H + \lambda I)^{-1} H^T y. \tag{7}$$

In the wavelet domain, the RLS can be formulated as

$$\hat{\tilde{x}} = \arg\min_{\tilde{x}} \{\|\tilde{H}\tilde{x} - \tilde{y}\|^2 + \lambda\|\tilde{x}\|^2\} \tag{8}$$

with the solution given by

$$\hat{\tilde{x}} = (\tilde{H}^T \tilde{H} + \lambda I)^{-1} \tilde{H}^T \tilde{y}. \tag{9}$$

C. 2-D Separable Wavelet Representation

For notational simplicity we will assume both X and Y are square images. Suppose x and y in (1) are vectors obtained from 2-D $N \times N$ image X and $M \times M$ image Y in the lexicographic order. Let W_x and W_y represent 1-D transform matrices for X and Y, respectively. Define $W_{M^2} = W_y \otimes W_y$ and $W_{N^2}^T = W_x^T \otimes W_x^T$, then similar to the 1-D case, we have

$$\tilde{H} = W_{M^2} H W_{N^2}^T, \quad \tilde{y} = W_{M^2} y, \quad \tilde{x} = W_{N^2} x. \tag{10}$$

Substituting $\tilde{H}$, $\tilde{y}$, and $\tilde{x}$ into (9), we can have the RLS solution in the 2-D wavelet domain. The question is how to calculate the four–dimensional wavelet transform $\tilde{H} =$
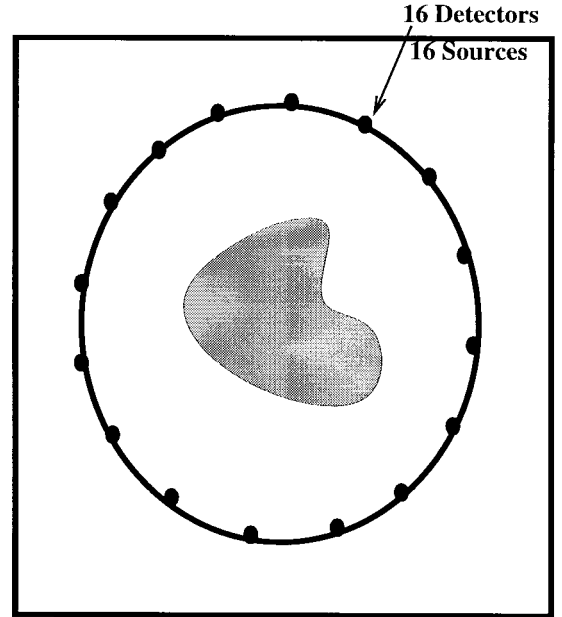

Fig. 3.　The source-detector configurations of the cylindrical rod.

$W_{M^2} H W_{N^2}^T$. Slightly different from [17], we do the following. First, for each row h_{r_i}, $i = 1, 2, \cdots, M^2$, of H, we reorder it to a 2-D image of size $N \times N$ and then use W_x to perform separable transform. After this separable transformation, we reorder the transformed image back to a row vector $\tilde{h}_{r_i}$. Let the resulting image be $\tilde{H}_r = HW_{N^2}^T$. Then, for each column of $\tilde{H}_r$, $\tilde{h}_{c_j}$, $j = 1, 2, \cdots, N^2$, we perform $W_{M^2}\tilde{h}_{c_j}$ in the form of $W_y \tilde{H}_{c_j, 2-D} W_y$, $j = 1, 2, \cdots, N^2$, where $\tilde{H}_{c_j, 2-D}$ is the 2-D ordering of $\tilde{h}_{c_j}$. Finally, we reorder the transformed vectors to a 2-D matrix which is $\tilde{H}$.

IV. MULTIGRID ALGORITHM

As we see from Section II, wavelet decomposition of a signal leads to a multiresolution representation of the signal. If we exploit the multiresolution property, the computational time may be reduced. In this paper, we employ a modified
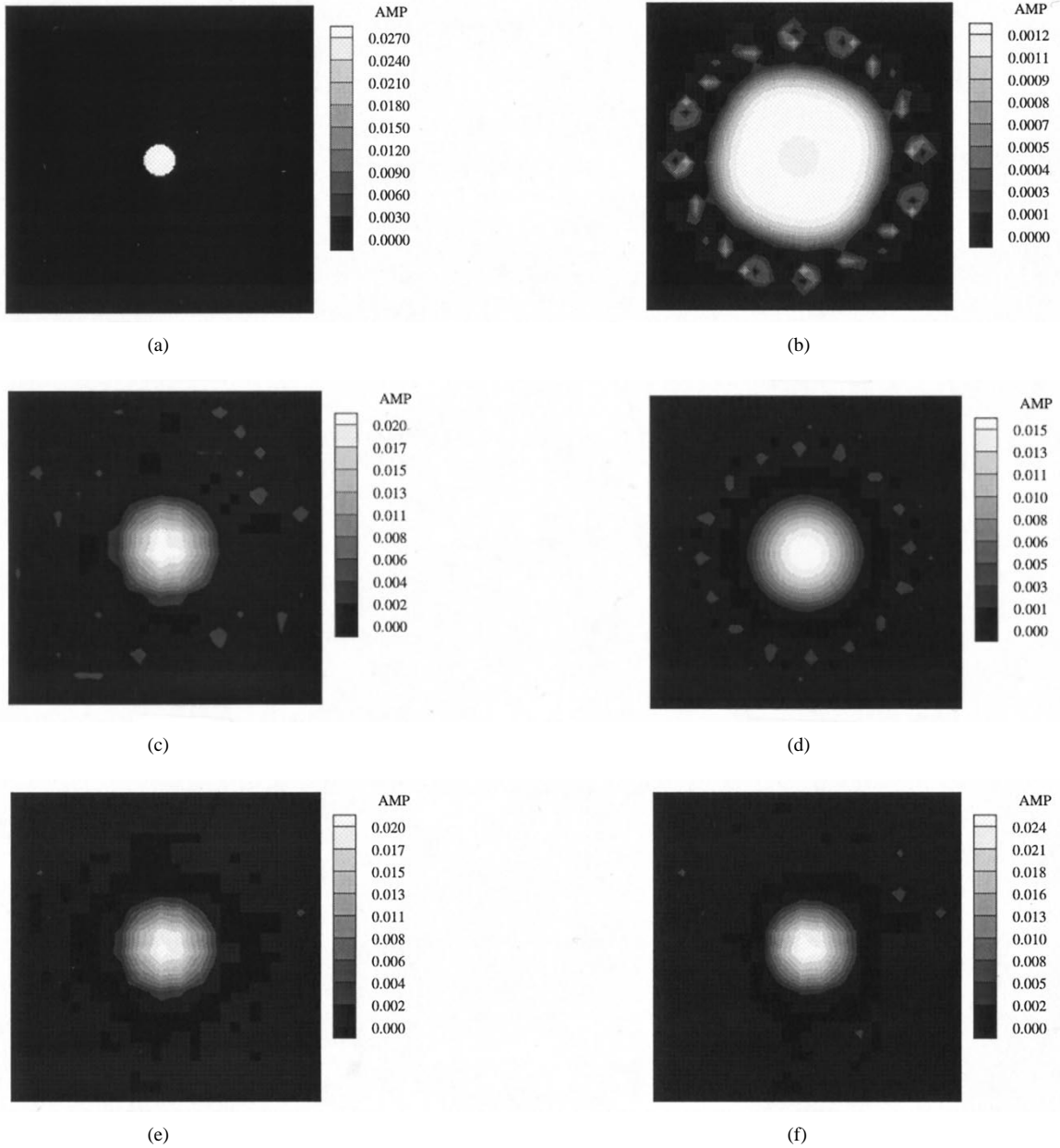
Fig. 4. Reconstruction results for a test medium containing a centered rod: (a) is the original object (difference between the absorption distribution of the test medium and a homogeneous background), (b) is the reconstructed object using one-grid CGD with 32 iterations, (c) is the reconstructed object using two-grid algorithm with 500 iterations in the coarse grid, (d) is the reconstructed object using one grid CGD with 235 iterations, (e) is the reconstructed object using the two-grid algorithm with additional 200 iterations in the fine grid, using (c) as initial solution, and (f) is the reconstructed object with 800 iterations in a localized region at the fine grid, also using (c) as the initial solution. The computation time for (b) and (c) are roughly same. So are (d), (e) and (f). The time for (c) is about 1/7 of (d).

V-cycle multigrid algorithm. The principle of this algorithm is illustrated in Fig. 2. There are two differences compared to the classical V-cycle method [18]. First, instead of downward (from fine to coarse) restriction, where error is calculated and restricted, here we use wavelet decomposition to reach the vertex (coarsest grid) of the V-cycle. For the upward reconstruction (form coarse to fine), we use multigrid reconstruction instead of error prolongation (error compensation). Let L represent the level of wavelet decomposition, this modified V-cycle algorithm consists of the following steps.

1) Perform wavelet transform of $\boldsymbol{y}$ and $\boldsymbol{H}$ to obtain $\tilde{\boldsymbol{y}}_l$ and $\tilde{\boldsymbol{H}}_l$, $l = -1, -2, \cdots, -L$. Set $l = -L$ and select an initial solution $\hat{\tilde{\boldsymbol{x}}}_{-L,0} = \mathbf{o}$.

2) Solve for the RLS solution $\hat{\tilde{\boldsymbol{x}}}_l$ of the perturbation equation at the lth level, $\tilde{\boldsymbol{H}}_l \tilde{\boldsymbol{x}}_l = \tilde{\boldsymbol{y}}_l$, using the CGD algorithm, with $\tilde{\boldsymbol{x}}_{l,0}$ as the initial solution.

3) Obtain the initial solution in the $(l+1)$th grid by prolongating from $\tilde{\boldsymbol{x}}_l$ to $\tilde{\boldsymbol{x}}_{l+1}$ through padding zeros, i.e., $\tilde{\boldsymbol{x}}_{l+1,0} = [\hat{\tilde{\boldsymbol{x}}}_l^T, \mathbf{o}^T]^T$.

4) Let $l = l + 1$, if $l = 0$, solve $\boldsymbol{H}x = \boldsymbol{y}$ using $\boldsymbol{W}^T \tilde{\boldsymbol{x}}_{0,0}$ as the initial solution. Otherwise, go back to Step 2.

The wavelet-based multigrid RLS algorithm described above differs from the one proposed by Wang *et al.* [11] in several aspects. First, in that method, at each resolution level, the LL, LH, HL, and HH components are reconstructed
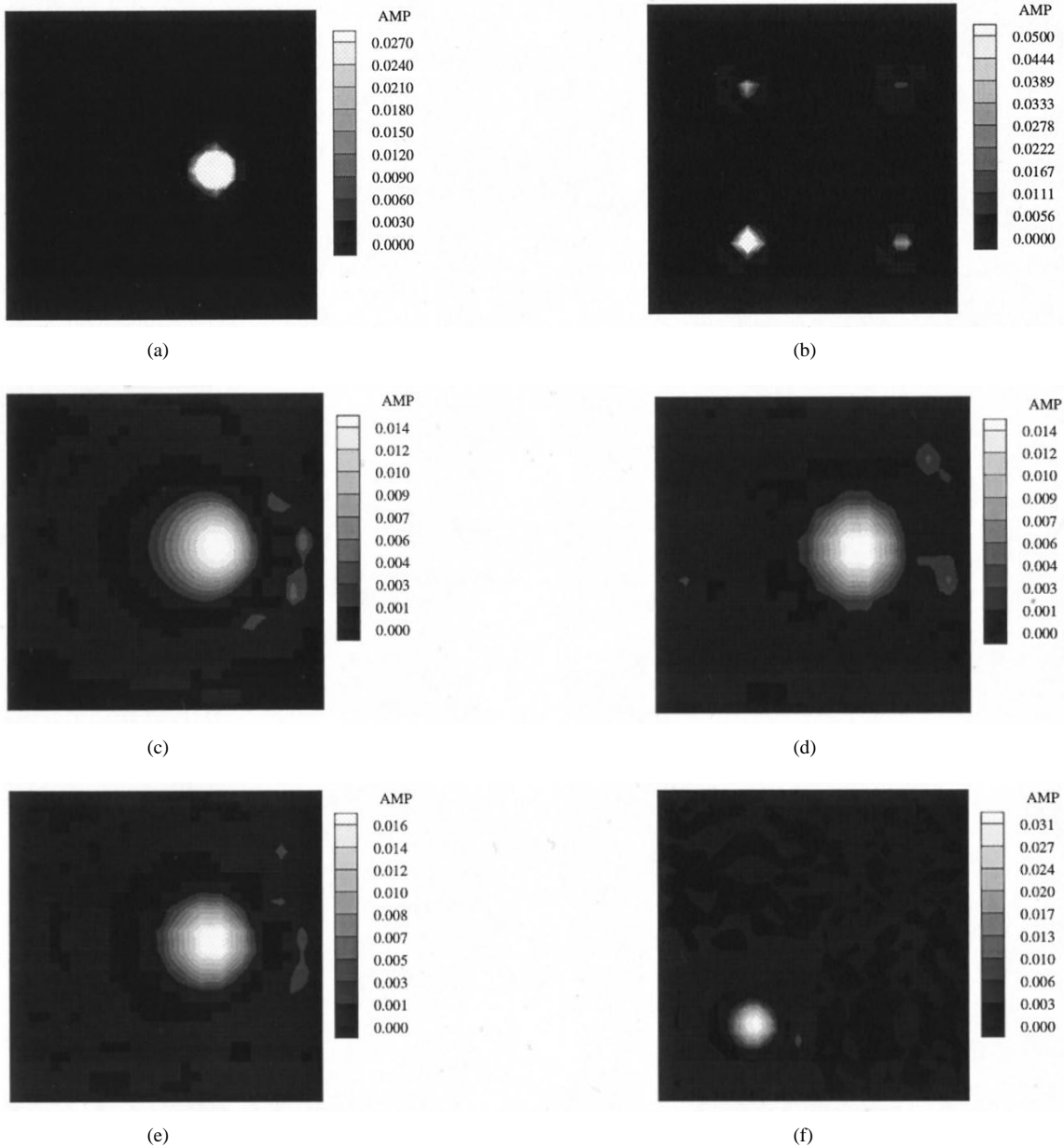
Fig. 5. Reconstruction results and wavelet analysis of a medium with an off-center rod with Sine-like distribution: (a) is the original object, (b) shows the wavelet transform of original object in (a), (c) is the reconstructed object using one grid with 235 iterations, (d) is the reconstructed object using two-grids algorithm with 500 iterations in the coarse grid, (e) is the reconstructed object using two-grid algorithm with additional 200 iterations in the fine grid, and (f) is the wavelet transform of (e). The total computation time for (e) and (c) are roughly the same. The time for (d) is about 1/7 of (c).

alternatingly until the solution converges. In our method, at each level, the LL component only is solved, assuming the other components are zeros. Second, in the method of [11], the regularization parameter is fixed at different resolutions. In our scheme, the regularization parameters at different grids (resolutions) are varied. In the coarsest resolution the noise is quite weak compared to the signal, so we do not need to apply much regularization. When the resolution goes from coarse to fine the regularization parameter is increased. This is because the noise is more pronounced in high frequencies.

In clinical applications, usually only certain regions with abnormal features are of interest. The above multigrid algorithm allows one to "zoom-in" special regions of interest (ROI's). Let's say we are interested in a region that appears "questionable" in a coarser level reconstruction. Then, only the corresponding region in the next finer resolution need to be further refined by the CGD algorithm, while other regions can be kept the same as in the previous coarser resolution.

Currently, we have only implemented a two-grid algorithm $(L = 1)$ by which we first reconstruct the LL component of the wavelet transform $\tilde{x}$ of x. This yields the coarse level reconstruction $\tilde{x}_{-1}$. Starting from this solution, we then solve all the components of $\tilde{x}$ or selected ROI's.

V. NUMERICAL SIMULATION RESULTS

In our current implementation, we have only considered imaging of absorption coefficients, assuming the scattering property of the target medium is the same as that of the back-

ground. In our simulation, the length-4 Daubechies' wavelet [19] is used because it achieves a good tradeoff between computational precision and computational complexity. In order to demonstrate the effectiveness of the wavelet-based multigrid RLS algorithm compared to a one-grid algorithm, two sets of simulations are performed. In the first simulation, a 1-cm-diameter rod is placed in a background medium which is infinite and homogeneous. The rod is homogeneous, with absorption and scattering coefficients $\mu_a = 0.05$ cm^{-1} and $\mu_s = 10$ cm^{-1}. The background medium has $\mu_a^b = 0.02$ cm^{-1} and $\mu_s^b = 10$ cm^{-1}. A total of 16 sources and 16 detectors are evenly spread about the rod in a ring geometry having a diameter of 10 cm (see Fig. 3). Solution to the forward problem (i.e., elements of $\boldsymbol{H}$ and $\boldsymbol{y}$) was accomplished by analytically solving the diffusion equation using the normal mode series method described in [20]. The data (i.e., elements of $\boldsymbol{y}$) consist of the difference in the forward-calculated continuous wave (CW) signal for the homogeneous medium and the medium containing the cylindrical rod. The reconstructed object (i.e., elements of $\boldsymbol{x}$) consists of the differences in the absorption coefficients of the real test medium and those of the background. Fig. 4 shows the reconstructed objects using one-grid and two-grid algorithms, respectively. The coarse level reconstruction only solves a quarter of the pixels in the fine resolution. Because the CGD algorithm requires $O(L^2)$ operations where L is the number of unknowns, one iteration of the coarse level takes 1/16 of the computation time of one iteration in the fine resolution. The comparison of the computation times indicated in the figure caption is derived based on this assumption. From Fig. 4, we see that the proposed multigrid algorithm can obtain significantly better reconstruction than the one-grid method under similar computation time [compare Fig. 4(b) and (c), also compare Fig. 4(d) and (e)], or require significantly shorter time to reach the same resolution quality [compare Fig. 4(c) and (d)]. Fig. 4(f) is obtained by restricting reconstruction in the fine grid within a ROI selected based on the coarse grid resolution. The ROI we used here is a square block (a quarter of the size of the original image domain) containing the rod at the center. Because more iterations can be performed under the same total time, it yields a quantitatively more accurate result than Fig. 4(e). In our reconstruction, we do not put any constraints on the range of $\boldsymbol{x}$. Therefore, some reconstruction values could be negative, which are set to zeros at the final step of the reconstruction.

In the second simulation a 1.5-cm-diameter rod is placed at an off-center position with respect to the source and detector ring. The rod has a nonhomogeneous absorption distribution, following a sinusoidal pattern (one positive cycle only) whose maximum value for μ_a is 0.05 cm^{-1}. The forward solution in this simulation is obtained by a multigrid finite difference solver described in [4]. Fig. 5 is the reconstruction results of the off-center case. We also show the wavelet decomposition of the original image and the final reconstructed image. From this figure, we can see that we can obtain quite accurate results from the coarse level reconstruction alone [see Fig. 5(d)]. This is because the energy of the original image is mostly contained in the LL band. This energy compaction property of
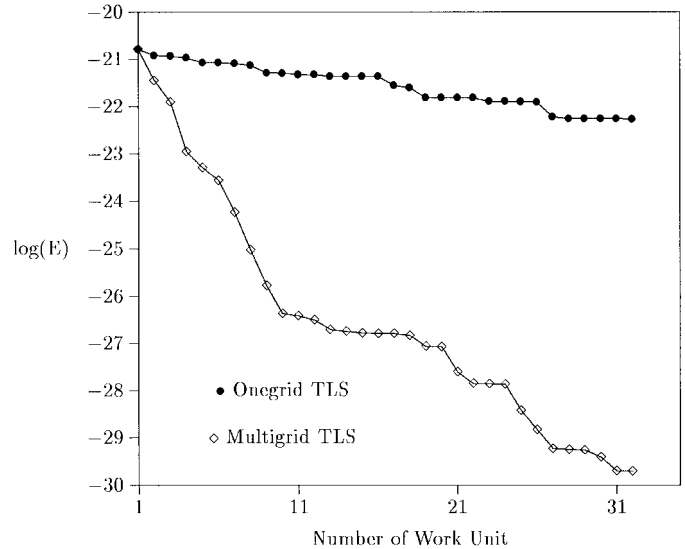

Fig. 6. Comparison of error reduction rates of multigrid versus one-grid RLS. Here, $E = \frac{1}{L}\|\boldsymbol{H}x - \boldsymbol{y}\|^2$ and one work unit is the computation time required for one iteration in the finest grid.

the wavelet transform makes the reconstruction in the wavelet domain more efficient for images that are smooth. To evaluate the savings of the computation times by the multigrid over the single-grid algorithm, Fig. 6 compares the values of the error function in (6) (at log scale) after successive numbers of work units obtained using the one-grid and two-grids methods. A work unit here is defined as the amount of computation for performing one iteration in the finest grid [21]. In plotting this curve, we have assumed that one coarse iteration takes 1/16 work unit. It can be seen that the multigrid method requires significantly fewer work units to reach the same error. It also reaches a lower minimum upon convergence.

In the above examples, the calculated data from the forward solution were used and the regularization parameter was set to zero. Next, we show the results when the data are corrupted by white Gaussian noise, with a signal-to-noise ratio (SNR) of 20 dB. Fig. 7 compares the reconstruction results with and without regularization in each grid. The regularization parameter was also chosen roughly based on the Miller criterion, followed by slight manual tuning. The regularization parameter in the coarse grid is one magnitude smaller than that in the fine grid. From these results, we can see that the use of regularization is more efficient in the fine grid [compare Fig. 7(c) and (e)]. Further, we also see that if we impose regularization in both coarse grid and fine grid we can get improved reconstruction in both grids.

VI. CONCLUSION AND DISCUSSION

In this paper, a wavelet-based multiresolution RLS reconstruction scheme is proposed to solve the perturbation equation used to compute images of the internal properties of a random scattering medium. Compared to the one-grid method, we have demonstrated that the proposed method can produce images of comparable or improved quality and accuracy at much lower computation costs. We have also shown that incorporation of regularization in the wavelet domain can effectively suppress
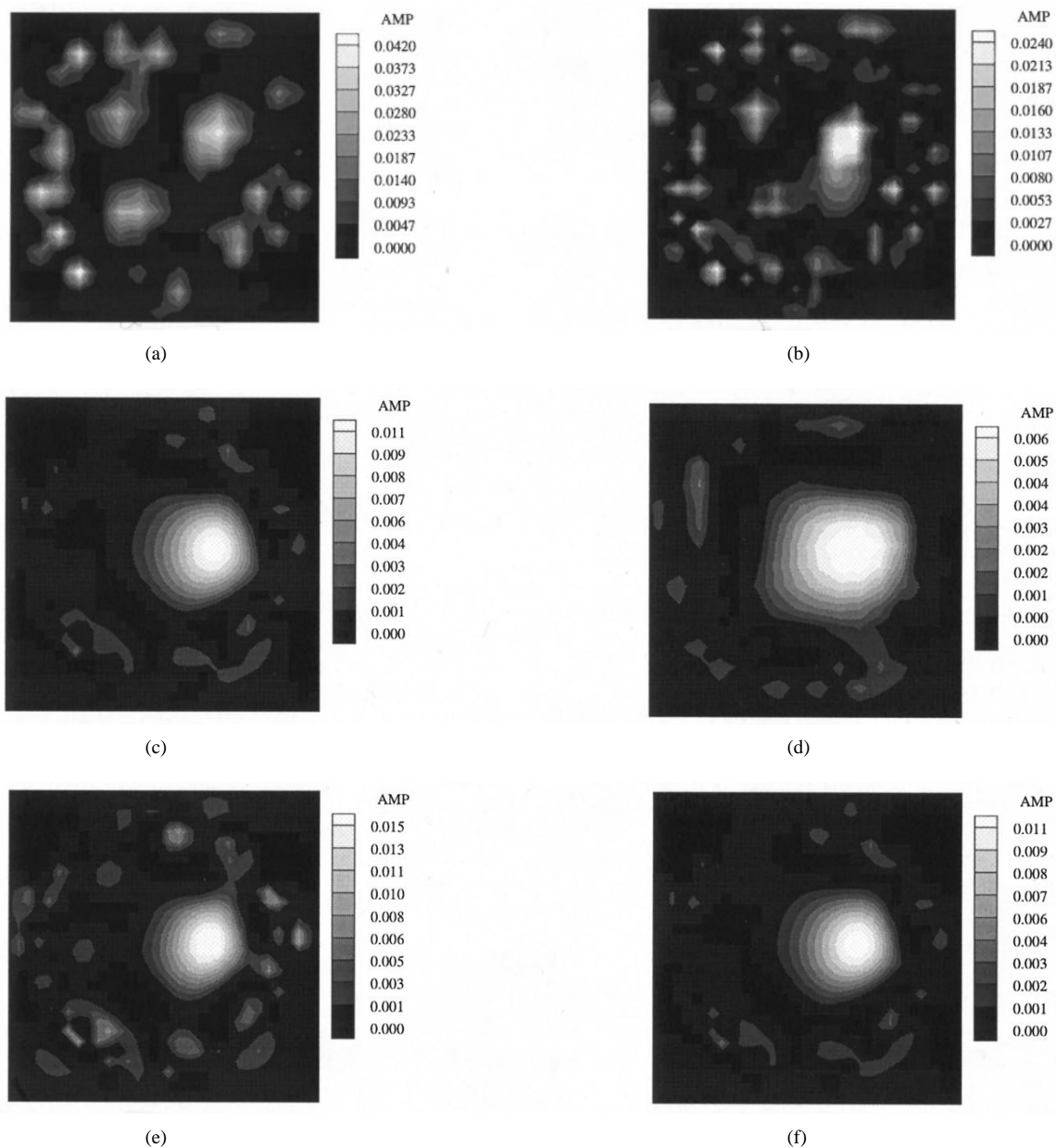
Fig. 7.   The reconstruction results for the object shown in Fig. 6(a) when the SNR is 20 dB: (a) is the reconstructed object with 500 iterations in the coarse grid without regularization, (b) is the reconstructed object with additional 200 iterations in the fine grid without regularization using (a) as an initial solution, (c) is the reconstructed object with additional 200 iterations in the fine grid with regularization also using (a) as an initial solution, (d) is the reconstructed object with 500 iterations in the coarse grid with regularization, (e) is the reconstructed object with additional 200 iterations in the fine grid without regularization using (d) as an initial solution, and (f) is the reconstructed object with additional 200 iterations in the fine grid with regularization using (d) as an initial solution.

image degradation caused by added noise. A point of further study will be to develop criteria and strategies for selection of regularization parameters at different scales.

Incorporation of multiresolution methods map well to examining selected ROI's without the need, and added computing effort, to evaluate the entire domain. Selected regions can be based on *a priori* knowledge and/or on determination of anomalies present in solutions obtained at a coarse grid. Subsequent focusing on a ROI on a finer grid invokes the assumption that computed coefficients in other regions are accurate. While this may prove useful for examination of simply structured media, its use with arbitrary media will require careful implementation especially if quantitatively accurate results are desired.

Development of practical methods for imaging thick tissue structures using optical sources will require balancing the needs of accuracy and resolution against the cost of computation. The method described here would seem to fit well with this requirement. It is also appreciated that the accuracy of computed solutions and the speed of convergence can often be significantly improved by the availability of prior knowledge. In this regard it would be of interest to assist the approach described here with anatomical priors that can be acquired using magnetic resonance (MR) imaging. We mention this because of the apparent practicality of performing optical measurements within an MR magnet. We also note that because the physical parameters being measured by MR

and optical methods are very different, information derived from a combined measurement might be expected to aid synergistically in diagnostic studies. In fact, we have recently demonstrated, using single grid solvers, the ability to recover qualitatively accurate images of simulated inclusions added to MR derived maps of female breast [22]. These studies also modeled time-independent optical sources. Further study is needed to explore adaptation of the described scheme to evaluate MR derived anatomical maps, and examine the possibility of focusing on ROI's identified from the MR image. ROI's could also be chosen based on converged solutions achieved on a coarse grid. If necessary, additional improvements in image accuracy could be obtained by computing iterative forward-inverse solutions on the coarse grid before computing solutions to ROI's on finer grids.

REFERENCES

[1] G. Müller *et al.*, *Medical Optical Tomography: Functional Imaging and Monitoring*, vol. SPIE-IS11. Bellingham, WA: SPIE, 1993.

[2] Y. Wang, J. Chang, R. Aronson, R. L. Barbour, H. L. Graber, and J. Lubowsky, "Imaging scattering media by diffusion tomography: An iterative perturbation approach," in *Proc. SPIE Conf. Physiological Monitoring and Early Detection Diagnostic Methods*, vol. SPIE-1641, Jan. 1992, pp. 58–71.

[3] R. L. Barbour, H. L. Graber, Y. Wang, J. Chang, and R. Aronson, "A perturbation approach for optical diffusion tomography using continuous-wave and time-resolved data," *Medical Optical Tomography—Functional Imaging and Monitoring*, vol. SPIE-IS11, pp. 87–120, 1993.

[4] Y. Q. Yao, Y. Wang, Y. L. Pei, W. Zhu, J. H. Hu, and R. L. Barbour, "Frequency domain optical tomography in human tissue," in *Proc. SPIE Conf. Experimental and Numerical Methods for Solving Ill-posed Inverse problems: Medical and Nonmedical Application*, July, 1995, vol. SPIE-2570.

[5] J. R. Singer *et al.*, "Image reconstruction of the interior of bodies that diffuse radiation," *Sciences*, vol. 248, pp. 990–993, 1990.

[6] S. R. Arridge *et al.*, "New results for the development of infrared-red absorption imaging," *SPIE Proc. Biomedical Image Processing*, 1990, vol. 1245, pp. 92–103.

[7] S. R. Arridge, "The forward and inverse problems in time resolved infra-red imaging," *SPIE Medical Optical Tomography—Functional Imaging and Monitoring*, vol. SPIE-IS11, pp. 35–64, 1993.

[8] J. Chang, Y. Wang, R. Aronson, H. L. Graber, and R. L. Barbour, "A layer-stripping approach for recovery of scattering media from time-resolved data," in *Proc. SPIE Conf. Inverse Problems in Scattering and Imaging*, July 1992, vol. SPIE-1767, pp. 384–395.

[9] W. Zhu, Y. Wang, H. L. Graber, R. L. Barbour, and J. Chang, "A regularized progressive expansion algorithm for recovery of scattering media from time-resolved data," in *Proc. of OSA Topical Meeting on Advances in Optical Imaging and Photon Migration*, Mar. 1994, pp. 211–216.

[10] W. Zhu, Y. Wang, J. Chang, H. L. Graber, and R. Barbour, "A total least squares approach for the solution of the perturbation equation," in *Proc. SPIE Conf. Optical Tomography, Photon Migration, and Spectroscopy of Tissue and Model Media*, Feb. 1955, vol. SPIE-2389, pp. 420–430.

[11] G. Wang, J. Zhang, and G. W. Pan, "Solution of inverse problems in image processing by wavelet expansion," *IEEE Trans. Image Processing*, vol. 4, no. 5, pp. 579–593, 1995.

[12] A. H. Delaney and Y. Bresler, "Multiresolution tomographic reconstruction using wavelets," *IEEE Trans. Image Processing*, vol. 6, no. 4, pp. 799–813, 1995.

[13] S. G. Mallat, "A theory for multiresolution signal decomposition: The wavelet representation," *IEEE Trans. Pattern Anal. Machine Intell.*, vol. 11, no. 7, pp. 674–693, 1989.

[14] A. N. Tikhonov and V. Y. Arsenin, *Solution of Ill-Posed Problems*. New York: Wiley, 1977.

[15] K. Miller, "Least squares method for ill–posed problems with a prescribed bound," *SIAM J. Math. Anal.*, vol. 1, pp. 52–74, Feb. 1970.

[16] G. H. Golub, M. Heath, and G. Wahba, "Generalized cross-validation as a method for choosing a good ridge parameter," *Technometrics*, vol. 21, no. 2, pp. 215–223, 1979.

[17] L. Blanc-Feraud, P. Charbonnier, P. Lobel, and M. Barlaud, "A fast tomographic reconstruction algorithm in the 2-D wavelet transform domain," in *Proc. IEEE Int Conf. Acoustics, Speech, Signal Processing (ICASSP'94)*, 1994, vol. V, pp. 305–308.

[18] W. Hackbusch, *Multigrid Methods and Applications*. Berlin, Germany: Springer-Verlag, 1985.

[19] W. H. Press, S. A. Teukolsky, W. T. Vetterling, and B. P. Flannery, *Numerical Recipes in C: The Art of Scientific Computing*, 2nd ed. Cambridge, U.K.: Cambridge Univ, 1992.

[20] Y. Q. Yao, Y. Wang, R. L. Barbour, H. L. Graber, and J. W. Chang, "Scattering characteristics of photon density waves from an object in a spherically two-layer medium," in *Proc. SPIE Conf. Optical Tomography, Photon Migration, and Spectroscopy of Tissue and Model Media*, Feb. 1995, vol. SPIE-2389, pp. 291–303.

[21] W. L. Briggs, *A Multigrid Tutorial*. Philadelphia, PA: SIAM, 1987.

[22] R. L. Barbour, H. L. Graber, J. Chang, S. Barbour, P.C. Koo, and R. Aronson, "MR guided optical tomography: Prospects and computation for a new imaging method," *IEEE Computational Science Engineering*, pp. 63–77, Winter 1995.